https://doi.org/10.5194/gmd-2020-398
Preprint. Discussion started: 16 December 2020

Geoscientific Model Development Discussions

Grid-Stretching Capability for the GEOS-Chem 13.0.0 Atmospheric Chemistry Model

Liam Bindle[1,2], Randall V. Martin[1,2,3], Matthew J. Cooper[2,1], Elizabeth W. Lundgren[4], Sebastian D. Eastham[5], Benjamin M. Auer[6], Thomas L. Clune[6], Hongjian Weng[7], Jintai Lin[7], Lee T. Murray[8], Jun Meng[2,1,9], Christoph A. Keller[6,10], Steven Pawson[6], and Daniel J. Jacob[4]

[1]Department of Energy, Environmental and Chemical Engineering, Washington University, St. Louis, Missouri, USA
[2]Department of Physics and Atmospheric Science, Dalhousie University, Halifax, NS, Canada
[3]Harvard-Smithsonian Centre for Astrophysics, Cambridge, MA, USA
[4]John A. Paulson School of Engineering and Applied Sciences, Harvard University, Cambridge, MA, USA
[5]Laboratory for Aviation and the Environment, Massachusetts Institute of Technology, Cambridge, MA, USA
[6]Global Modeling and Assimilation Office, NASA Goddard Space Flight Center, Greenbelt, MD, USA
[7]Laboratory for Climate and Ocean–Atmosphere Studies, Department of Atmospheric and Oceanic Sciences, School of Physics, Peking University, Beijing, China
[8]Department of Earth and Environmental Sciences, University of Rochester, Rochester, NY, USA
[9]Atmospheric and Oceanic Sciences, University of California, Los Angeles, Los Angeles, California, USA
[10]Universities Space Research Association, Columbia, MD, USA

Correspondence: Liam Bindle (liam.bindle@wustl.edu)

Abstract. Modeling atmospheric chemistry at fine resolution globally is computationally expensive; the capability to focus on specific geographic regions using a multiscale grid is desirable. Here, we develop, validate, and demonstrate stretched-grids in the GEOS-Chem atmospheric chemistry model in its high performance implementation (GCHP). These multiscale grids are specified at runtime by four parameters that offer users nimble control of the region that is refined and the resolution of the refinement. We validate the stretched-grid simulation versus global cubed-sphere simulations. We demonstrate the operation and flexibility of stretched-grid simulations with two case studies that compare simulated tropospheric NO_2 column densities from stretched-grid and cubed-sphere simulations to retrieved column densities from the TROPOspheric Monitoring Instrument (TROPOMI). The first case study uses a stretched-grid with a broad refinement covering the contiguous US to produce simulated columns that perform similarly to a C180 (∼50 km) cubed-sphere simulation at less than one-ninth the computational expense. The second case study experiments with a large stretch-factor for a global stretched-grid simulation with a highly localized refinement with ∼10 km resolution for California. We find that the refinement improves spatial agreement with TROPOMI columns compared to a C90 cubed-sphere simulation of comparable computational demands, despite conducting the simulation at a finer resolution than parent meteorological fields. Overall we find that stretched-grids in GEOS-Chem are a practical tool for fine resolution regional- or continental-scale simulations of atmospheric chemistry. Stretched-grids are available in GEOS-Chem version 13.0.0.

https://doi.org/10.5194/gmd-2020-398
Preprint. Discussion started: 16 December 2020

Geoscientific Model Development Discussions

1 Introduction

Global simulations of atmospheric chemistry are computationally demanding. Chemical mechanisms in the troposphere typically involve more than 100 chemical species, emitted by anthropogenic and natural sources, mixing through 3-D transport on all scales. Typical global model resolutions are on the order of hundreds of kilometers and generally limited by the availability of computational resources. Massively parallel models such as GEOS-Chem in its high-performance implementation (GCHP; Eastham et al. (2018)) can run on more than 1000 cores (Zhuang et al., 2020) with demonstrated capability of 50 km resolution. The coarse resolution of global models can lead to systematic errors in applications when scales of variability finer than the model resolution are relevant, such as vertical transport and scavenging by convective updrafts (Mari et al., 2000; Li et al., 2018, 2019), nonlinear chemistry such as NO_x titration (Valin et al., 2011), localized emission sources (Davis et al., 2001; Freitas et al., 2007), a priori profiles for satellite retrievals (Heckel et al., 2011; Goldberg et al., 2017; Kim et al., 2018), and simulated concentrations for population exposure estimates (Punger and West, 2013; Li et al., 2016). Nested grids are commonly used for simulations that need to capture fine-scale modes of variability. With one-way nested grids, a global simulation generates boundary conditions for a fine resolution regional simulation (Wang et al., 2004; Lin et al., 2020). With two-way nested grids, the global simulation is dynamically coupled to the regional simulation (Yan et al., 2014; Feng et al., 2020). An alternative type of multiscale grids that are well-established in the regional climate modeling community are stretched-grids (Fox-Rabinovitz et al., 2006, 2008). Stretched-grids are deformed model grids with increased grid density in the region of interest, and transition smoothly between the refinement and coarser global resolutions. Stretched-grids have the advantage of being inherently two-way coupled, and since stretching does not change the grid topology, grid-independent models like GEOS-Chem can implement stretched-grids without structural changes or online simulation couplers. Stretched-grid simulations have little overhead and are economical because their computational cost is similar to a cubed-sphere simulation with the same grid size. Here we implement, validate, and demonstrate stretched-grids in GEOS-Chem, enabling massively parallel global multiscale simulations of atmospheric chemistry.

Several recent works set the stage for the development of grid-stretching in GEOS-Chem. Long et al. (2015) developed the grid-independent capability of GEOS-Chem. Harris et al. (2016) developed the capability for stretched-grids in the GFDL Finite-Volume Cubed-Sphere Dynamical Core (FV3), which GCHP uses to calculate advection. Eastham et al. (2018) developed the capability for GEOS-Chem to operate on cubed-sphere grids in a distributed memory framework for massive parallelization, and to use the Model Analysis and Prediction Layer (MAPL) of the NASA Global Modeling and Assimilation Office (GMAO) together with the Earth System Modeling Framework (ESMF) to couple model components. GEOS-Chem version 12.5.0 added grid-independent emissions that produce consistent emissions regardless of the model grid (Weng et al., 2020; The International GEOS-Chem User Community, 2019). Most recently, MAPL version 2 (Thompson et al., 2020) of the NASA GMAO added stretched-grid support.

This manuscript describes the development and validation of the grid-stretching capability in GCHP and discusses practical considerations for running stretched-grid simulations. Sect. 2.1 provides an overview of GCHP and its underlying gnomonic cubed-sphere grid. Sect. 2.2 describes stretching the grid with the Schmidt (1977) transform following the methodology of

https://doi.org/10.5194/gmd-2020-398
Preprint. Discussion started: 16 December 2020


Geoscientific Model Development Discussions

Harris et al. (2016). Sect. 2.3 discusses considerations for stretched-grid simulations and a simple procedure for choosing an appropriate stretch-factor. Sect. 2.4 describes the model configuration for the simulations in the manuscript. Sect 2.5 summarizes the testing of stretched-grids in GCHP and provides a comparison of simulated oxidants and $PM_{2.5}$ concentrations from stretched-grid and cubed-sphere simulations. Sect. 3 presents two case studies that demonstrate and explore stretched-grid applications, with comparisons of stretched-grid and cubed-sphere simulations with observations from TROPOspheric Monitoring Instrument (TROPOMI).

2 Development of Stretched-Grids in GEOS-Chem

2.1 GEOS-Chem in its High-Performance Implementation (GCHP)

We use GEOS-Chem version 13.0.0 in its high-performance implementation (GCHP; Eastham et al. (2018)). GEOS-Chem, originally described in Bey et al. (2001), simulates tropospheric-stratospheric chemistry by solving 3-D chemical continuity equations. GCHP uses MAPL (Suarez et al., 2007) and ESMF (Hill et al., 2004), which facilitate the coupling of model components and the use of the High-Performance Computing (HPC) infrastructure. The 3-D advection component is the GFDL Finite-Volume Cubed-Sphere Dynamical Core (Putman and Lin, 2007). Columnar operators (Long et al., 2015) are used for columnar or local calculations such as convection and chemical kinetics. Emissions are aggregated, parameterized, and computed with the Harmonized Emissions Component (HEMCO) described in Keller et al. (2014). Offline meteorological data is from the Goddard Earth Observing System (GEOS) data assimilation system. All regridding, including the regridding of emissions data and meteorological data, is performed online by ESMF. GCHP discretizes the atmosphere with a gnomonic cubed-sphere grid with levels extending from the surface to 1 Pa. The cubed-sphere grid has several advantages over the conventional latitude-longitude grid, stemming from its more uniform grid-boxes that benefit the parallelization and numerical stability of transport (Eastham et al., 2018). The horizontal resolution of a GCHP simulation is a key determinant of its computational demands.

2.2 Grid-stretching

The grid-stretching procedure in GCHP, described here, uses a simplified form of the Schmidt transform for gnomonic cubed-sphere grids, and follows the methodology of Harris et al. (2016). The Schmidt (1977) transform can be applied to any grid, and effectively stretches the grid to increase its density in a region. The grid-stretching procedure has two steps and starts with a gnomonic cubed-sphere grid. First, the grid is refined at the South Pole by remapping the grid coordinate latitudes with a modified Schmidt transform

$$\phi'(\phi) = \arcsin\frac{D+\sin\phi}{1+D\sin\phi} \quad \text{where} \quad D=\frac{1-S^2}{1+S^2} \tag{1}$$

where ϕ is an input latitude, ϕ' is the output latitude, and S is a parameter called the *stretch-factor*. The stretch-factor controls the strength of this remapping operation, which effectively attracts the grid coordinates towards the South Pole along meridians. The second step is rotating the entire grid so that the refinement at the South Pole is repositioned to the region of interest. The

https://doi.org/10.5194/gmd-2020-398
Preprint. Discussion started: 16 December 2020

Geoscientific Model Development Discussions
Open Access
EGU

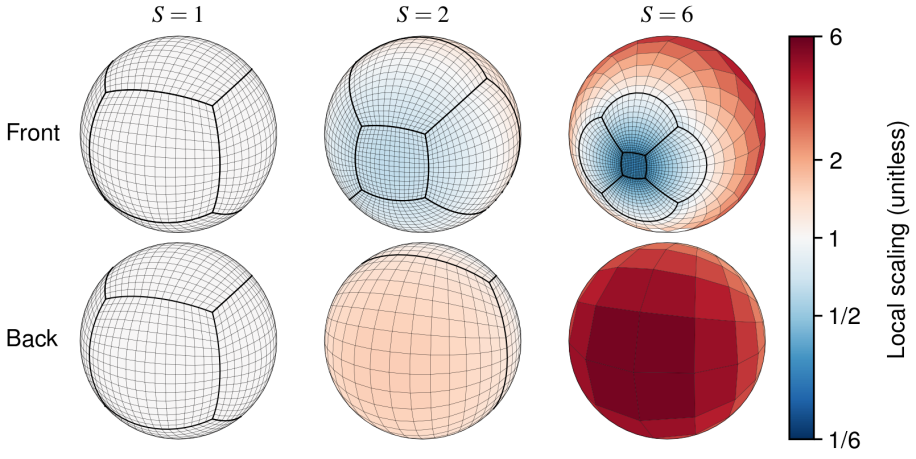

Figure 1. Three stretched-grids that illustrate the effect of the stretch-factor (S) on stretching a C16 cubed-sphere. Local scaling is the relative change to a grid-box's edge length induced by stretching.

user specifies a *target latitude* and *target longitude* (ϕ_t, θ_t), and the refinement is re-centered to this coordinate. In GCHP, according to the right-hand-rule, these rotations are $\phi_t + 90$ about 90 °E and $\theta_t + 180$ about 90 °N. Note that nonstretched cubed-sphere grids in GCHP have a -10 °E offset, so a stretched-grid with parameters $S = 1$, $\phi_t = -90$ °N, $\theta_t = 170$ °E is identical to a nonstretched cubed-sphere grid.

Figure 1 illustrates the effect of S on stretching a cubed-sphere grid. A stretch-factor greater than one causes stretching. Larger stretch-factors cause more stretching, and result in a finer and more localized refinement. The resolution at the center of the refinement is approximately S times finer than it was before stretching, and similarly, the antipode resolution is approximately S times coarser. These relative changes are approximate since the Schmidt transform is continuous and the grid-boxes have nonzero length edges. The grids in Figure 1 illustrate three noteworthy features of stretched-grids: (1) the changes in resolution are smooth, (2) the refined domain gets smaller as S increases, and (3) grid-boxes outside the refined domain expand. The cubed-sphere face at the center of the refined domain is called the *target-face*.

The relative change to a grid-box's size from stretching can be quantified by *local scaling*. This quantity represents the effect of grid-stretching at a given point. For a stretch-factor of S, the local scaling at a given point depends exclusively on how far that point is from the target coordinate. Local scaling, L, can be derived from Eqn. 1, and expressed as

$$L(\Theta; S) = \frac{1 + \cos\Theta + S^2(1 - \cos\Theta)}{2S} \tag{2}$$

where Θ is the angular distance to the target point. Appendix B contains the derivation of Eqn. 2. Figure 2 shows local scaling as a function of distance, for stretch-factors between 1 and 10. Overlaid are dashed lines that show the distance of cubed-sphere face edges after stretching. In the target-face, local scaling is approximately $1/S$ and nearly constant. Grid-stretching refines the resolution to the distance where $L = 1$, and coarsens the resolution at farther distances.

https://doi.org/10.5194/gmd-2020-398
Preprint. Discussion started: 16 December 2020

Geoscientific Model Development Discussions
Open Access
EGU

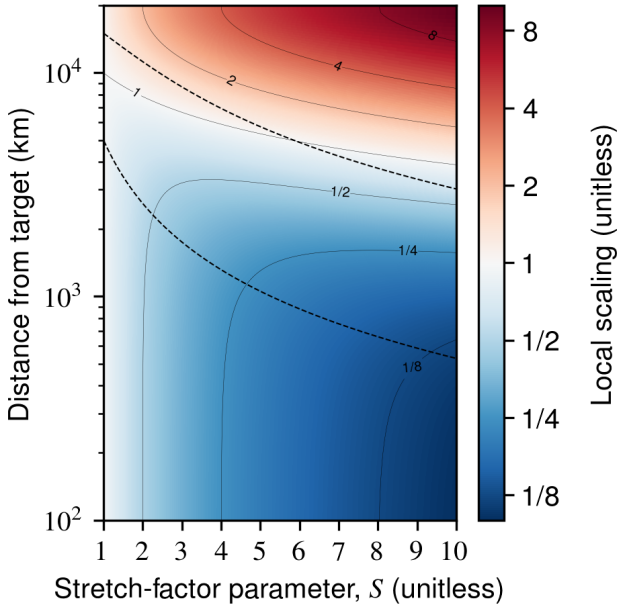

Figure 2. Local scaling as a function of distance from the target point, for stretch-factors in the range 1–10. The dashed lines show the distance from the target point to the cubed-sphere face edges after stretching. The lower dashed line is the distance to the center of the target-face's edges, and the upper dashed line is the distance to the center of the opposite face's edges.

Four scalar parameters fully describe a stretched-grid: the size of the cubed-sphere, the stretch-factor (S), the target latitude (ϕ_t), and the target longitude (θ_t). These concise parameters are conceptually simple, precise, and give the user nimble control of the grid. The combination of cubed-sphere size and stretch-factor controls the grid resolution. The target latitude and longitude specify the center of the refined domain. Moderate stretch-factors (e.g., 1.4–3.0) are suitable for broad refinements for continental-scale studies. Large stretch-factors (e.g., >5.0) are suitable for localized refinements for regional-scale studies.

2.3 Choosing an appropriate stretch-factor

Although the stretch-factor is a well-defined parameter, an appropriate value is application-specific and moderately variable. For computational efficiency, it is desirable to use the largest viable stretch-factor, to achieve the finest refinement for a given cubed-sphere size. However, larger stretch-factors also result in a smaller domain being refined and a coarser resolution at the target's antipode. To determine the maximum suitable stretch-factor for a given application, one should consider the size of the domain to be refined, and the sensitivity of the study species to coarse resolution outside the refined domain. It is also worth noting that there is limited prior model evaluation of GEOS-Chem at resolutions coarser than C24 (∼400 km). A simple procedure for choosing a stretch-factor, S, is choosing the maximum stretch-factor subject to two constraints:

1. **Constraining S by the size of the refined domain.** Local scaling is approximately constant and equal to $1/S$ throughout the target-face. Therefore, defining the refined domain as the region whose resolution is enhanced by a factor of $\sim S$, the

https://doi.org/10.5194/gmd-2020-398
Preprint. Discussion started: 16 December 2020


Geoscientific Model Development Discussions

target-face is a reasonable approximation of the refined domain. A constraint for S, such that the width of the target-face is greater than w_{tf}, is $S < 0.414 \cot(w_{tf}/4\, r_E)$ where r_E is Earth's radius. For example, for a refined domain with a diameter of at least 3000 km, $S < 3.5$. Alternatively, one can inspect Figure 2 to find the distance from the target point to the edge of the target-face for a given value of S.

2. **Constraining S by a maximum and minimum resolution.** The target resolution is S^2 times finer than the antipodal resolution; therefore, a constraint for S based on the desired maximum resolution, R_{max}, and minimum resolution, R_{min}, is $S < \sqrt{R_{max}/R_{min}}$. For example, for a maximum and minimum resolution comparable to a nonstretched C360 and C24 cubed-sphere, $S < 3.9$.

Once the constraints for S are determined, one can choose S and the grid size for their simulation. It is worth noting that GCHP requires that the grid size is an even integer (e.g., C88, C90, and C92). For example, for a stretched-grid with refined domain with a diameter greater than 3000 km, a maximum resolution of C360, and a minimum resolution of C24, the constraints would be $S < 3.5$ and $S < 3.9$. Then, one would choose a cubed-sphere size of C104 and $S = 3.46$.

2.4 Model configuration

All simulations in this manuscript use GCHP version 13.0.0-alpha.3 with a common configuration. Table 1 describes emissions for the US. We use monthly anthropogenic emissions based on the National Emission Inventory (NEI) for 2011 with updated annual scaling factors to account for changes in annual totals since 2011. In 2018, the scaling factor for NO was 0.64. Biomass burning emissions are from the Global Fire Emissions Database version 4 (GFED4). Aircraft emissions are from the Aviation Emissions Inventory Code (AEIC; Stettler et al. (2011)). We use inventories for NO_x emissions from soil microbial activity and lightning calculated offline at the native resolution of the meteorology (Weng et al., 2020; The International GEOS-Chem User Community, 2019). Offline soil NO_x emissions are based on the scheme described in Hudman et al. (2012), and offline lightning NO_x emissions are based on the scheme described in Murray et al. (2012). We use meteorological inputs from the GEOS-FP archive, which are archived on a $0.25° \times 0.3125°$ grid. We use a 10-minute timestep for chemistry and a 5-minute timestep for transport. The initial conditions for each simulation were regridded offline.

Simulations are named according to their grid. Nonstretched cubed-sphere simulations are named by their resolution with the suffix "-global", referring to their resolution being quasi-uniform globally. For example, a nonstretched C180 cubed-sphere simulation is named "C180-global". Stretched-grid simulations are named according to their refinement effective resolution, with a suffix denoting the region that is refined. For example, a stretched-grid simulation with an effective resolution of C180 in the contiguous US is named "C180e-US". "C180e" refers to the stretched-grid refinement being comparable to the resolution of a C180 cubed-sphere grid.

2.5 Stretched-grid development and validation

Developing and testing stretched-grids in GCHP involved multiple stages. The first step was developing a prototype simulation to confirm the functionality of grid-stretching in each model component. The prototype simulation excluded chemistry and

https://doi.org/10.5194/gmd-2020-398
Preprint. Discussion started: 16 December 2020

Geoscientific Model Development Discussions

Table 1. Simulation emission sources for the US.

Source type	Inventory	Resolution	Notes
Anthropogenic	NEI-2011	$0.1^\circ \times 0.1^\circ$	With updated annual totals for 2018[1]
Lightning	—	$0.25^\circ \times 0.3125^\circ$	Described in Murray et al. (2012)
Soil	—	$0.25^\circ \times 0.3125^\circ$	Described in Weng et al. (2020)
Biomass burning	GFED4	$0.25^\circ \times 0.25^\circ$	Monthly fluxes
Aircraft	AEIC	$1.0^\circ \times 1.0^\circ$	Described in Stettler et al. (2011)
Shipping	CEDS[2]	$0.5^\circ \times 0.5^\circ$	Described in McDuffie et al. (2020)

1. Monthly fluxes, including diurnal and weekday–weekend variations and vertical allocations, based on criteria pollutants National Tier 1 from https://www.epa.gov/air-emissions-inventories/air-pollutant-emissions-trends-data (Accessed May 8, 2020).
2. Community Emissions Data System (CEDS)

used a simplified set of emissions. Once the prototype simulation was operational, full chemsitry and the full set of emissions were enabled. Specialized benchmarking code was then used to compare stretched-grid and cubed-sphere simulations, to debug and test the implementation.

Next we compare the concentrations of oxidants and $PM_{2.5}$ from cubed-sphere and stretched-grid simulations. The domain for this comparison is the contiguous US, and a C96 cubed-sphere simulation was chosen as the control (C96-global). The stretched-grid simulation, C96e-NA, had a grid size of C48, and its parameters were chosen so its average resolution was the same as C96-global in the contiguous US. C96e-NA's parameters were $S = 2.4$, $\phi_t = 35^\circ$ N, and $\theta_t = 96^\circ$ W. Figure 3 compares the resolution of C96e-NA and C96-global grids. Note that the stretch-factor is 2.4, rather than 2.0, because the cubed-sphere's quasi-uniform resolution is finer in the US than its nominal global resolution. A consequence of C96e-NA and C96-global having similar resolution is that their grid-boxes have minimal overlap. This makes the comparison sensitive to the precision of upscaling emissions (i.e. differences in upscaled emissions like NO point sources from the differences in how the grids cover a region). To calibrate expected differences between C96e-NA and C96-global, we compare C96-global to a second cubed-sphere simulation, C94-global. The resolution difference between C96-global and C94-global is 2.1 %; C96-global and C94-global grid-boxes have minimal overlap (beat frequency of 2), and the only overlapping occurs at the edges and center lines of faces.

Figure 4 compares C96e-NA with C96-global, and C94-global with C96-global. These comparisons are done for the fourth simulation month, to accomodate relaxation time for CO and O_3. The scatter near the surface is caused by differences in the spatial allocation of emissions on different grids (the precision of upscaling). Figure 4 shows that simulated averages from C96e-NA are consistent with C96-global and that their differences are comparable to the differences between two similar cubed-sphere simulations.

https://doi.org/10.5194/gmd-2020-398
Preprint. Discussion started: 16 December 2020

Geoscientific Model Development Discussions
Open Access
EGU

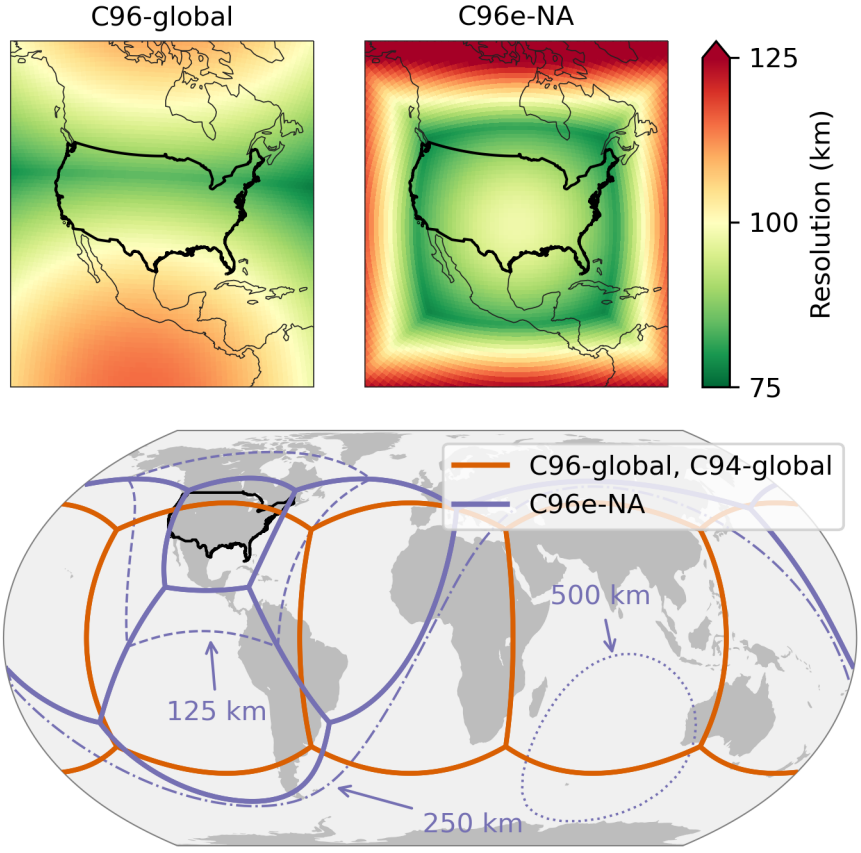

Figure 3. Comparison of C96-global and C96e-NA grids. The top panels show the variability of resolution for both grids. The bottom panel shows the grid face edges for C96-global and C96e-NA, with the 125 km, 250 km, and 500 km resolution contours for C96e-NA.

3 Stretched-Grid Case-Studies

Next, we focus on two case studies to further demonstrate the operation of stretched-grid simulations and the flexibility of stretched-grid refinements. The first is a typical case that considers a stretched-grid simulation with a moderate stretch-factor for a broad refinement covering the contiguous US at ∼50 km (C180e) resolution. The second is an exploratory case that experiments with a large stretch-factor for a localized refinement covering California at ∼10 km (C900e) resolution. The resolution of our second case study (∼10 km) is more than twice as fine as GEOS-Chem's native resolution of C360 (∼25 km) determined by the GEOS assimilated meteorological data.

We focus on NO_2 as a well measured species that is sensitive to resolution. Simulated tropospheric NO_2 column densities from stretched-grid and cubed-sphere simulations are compared to retrieved column densities from TROPOMI (Veefkind et al., 2012). TROPOMI is an instrument onboard the Sentinel-5P satellite launched in 2018 into a sun-synchronous orbit with a local overpass time of 13:30. TROPOMI includes ultraviolet and visible band spectrometers, and the retrieved NO_2 column

https://doi.org/10.5194/gmd-2020-398
Preprint. Discussion started: 16 December 2020

Geoscientific Model Development Discussions
Open Access
EGU

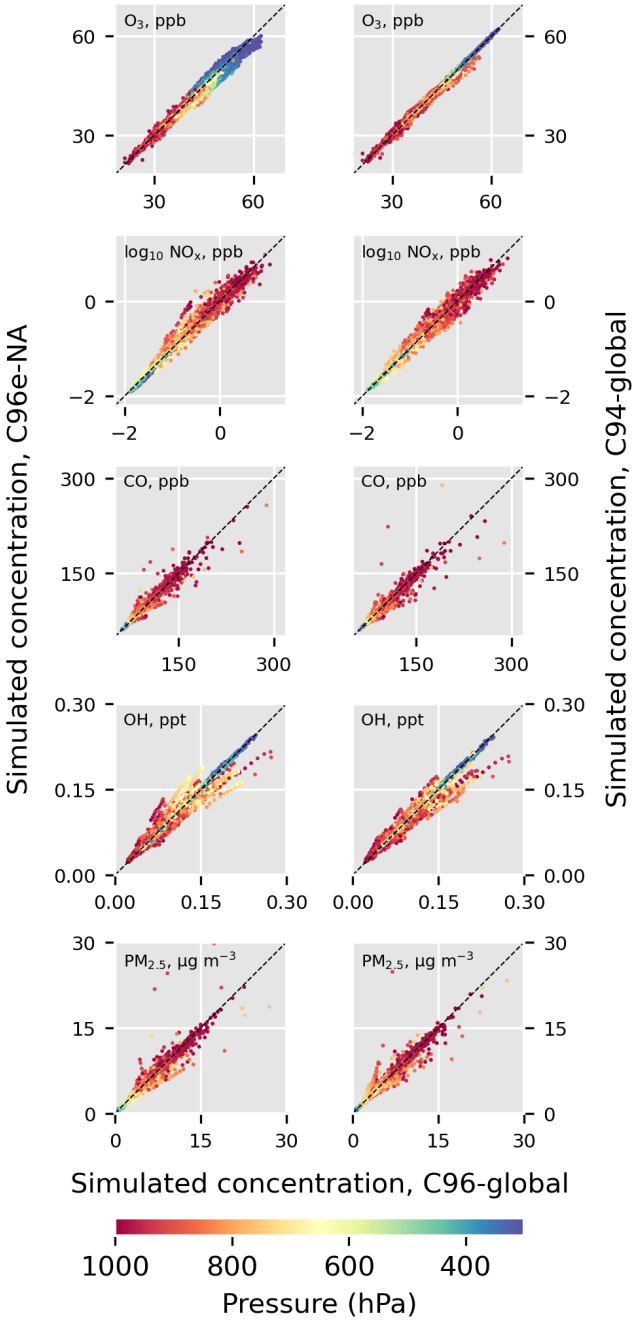

Figure 4. Comparison of simulated concentrations from C96e-NA with C96-global, and C94-global with C96-global. Points are 1-month time averages for each grid-box in the contiguous US for the fourth simulation month (September 2018). The right column gauges expected differences due to the precision of upscaling emissions to different grids.

https://doi.org/10.5194/gmd-2020-398
Preprint. Discussion started: 16 December 2020


Geoscientific Model Development Discussions

densities at 3.5×5.5 km^2 resolution use a modified version of the Dutch OMI NO_2 (DOMINO) retrieval algorithm (Boersma et al., 2011, 2018). We include observations with retrieved cloud fractions less than 10 %. Retrieved NO_2 column densities are sensitive to the a priori profiles used to calculate the air mass factors (Boersma et al., 2018; Lorente et al., 2017). To avoid spurious differences from the retrieval's a priori profiles when comparing simulated and retrieved NO_2 column densities, we recalculate the air mass factors with the mean simulated relative vertical profiles (shape factors) from the stretched-grid simulations following the approach described in Cooper et al. (2020) and Palmer et al. (2001). Evaluations of TROPOMI NO_2 columns show good correlation with ground-based measurements with a small low bias (Griffin et al., 2019; Ialongo et al., 2020; Zhao et al., 2020; Tack et al., 2020).

3.1 A stretched-grid simulation with a moderate stretch-factor

Stretched-grids with moderate stretch-factors have broad refinements and are well-suited for continental-scale simulation purposes. Here, we compare a global fine resolution C180 cubed-sphere simulation (C180-global) to a stretched-grid simulation with a moderate stretch-factor. This comparison focuses on the contiguous US. The stretched-grid simulation, C180e-US, has a grid size of C60 and parameters $S = 3.0$, $\phi_t = 36°$ N, and $\theta_t = 99°$ W. Figure 5 compares the grids of C180-global and C180e-US. For the contiguous US, the average resolution of C180-global is 47.9 km and the average resolution of C180e-US is 56.6 km. The two simulations have comparable resolution, but the cost of C180e-US is comparable to that of a C60 simulation; C180e-US has nine times fewer grid-boxes than C180-global. The coarsest resolution of C180e-US is approximately C20e in the southern Indian Ocean. In addition to C180-global and C180e-US, we conducted a C60 cubed-sphere simulation (C60-global) for comparison with C180e-US.

Figure 6 shows tropospheric NO_2 column densities from TROPOMI, C180-global, C180e-US, and C60-global for the US in July 2018. The three simulations included a 1-month spinup. The TROPOMI columns have high-concentrations over major cities and low NO_2 concentrations in rural and remote regions. Simulated NO_2 column densities from C180-global and C180e-US are consistent throughout the domain and generally capture the plumes over cities and the low concentrations in rural and remote areas. Small differences like those seen at the Four Corners, or near Denver, can be attributed the differences from upscaling NO point sources to the simulation grids. C60-global failed to resolve the local enhancements over major cities, and comparison with C180e-US highlights the effectiveness of grid-stretching.

The computational demands of C180e-US were significantly less than C180-global and comparable to C60-global. Table 2 gives timing test results for C180-global, C180e-US, and C60-global. The total CPU time for C180e-US was nearly a factor of 20 less than C180-global, resulting from fewer grid-boxes and reduced overhead. The total CPU time for C180e-US was 15 % greater than C60-global. The slight increase of data input cost in C180e-US is suspected to be caused by a load imbalance in online input regridding in ESMF. Work to mitigate this load imbalance is underway.

3.2 A stretched-grid simulation with a large stretch-factor

Stretched-grids with large stretch-factors have localized refinements. Here we experiment with a large stretch-factor to create a localized refinement covering California at ∼10 km resolution. Our focus on California is motivated by the pronounced

https://doi.org/10.5194/gmd-2020-398
Preprint. Discussion started: 16 December 2020

Geoscientific Model Development Discussions
Open Access
EGU

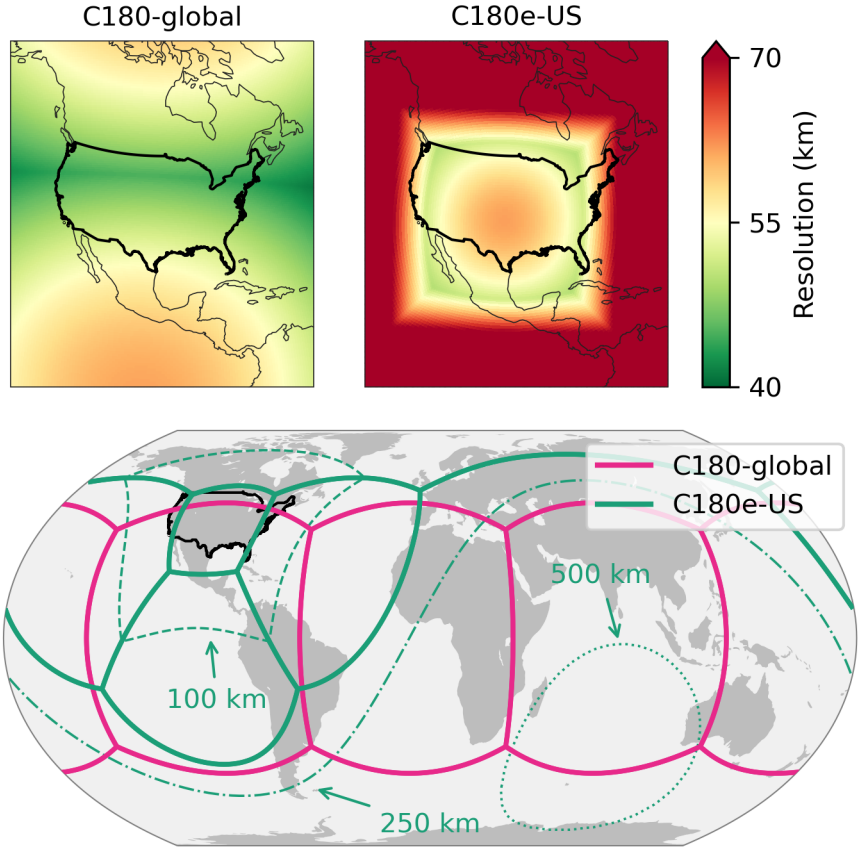

Figure 5. Comparison of C180-global and C180e-US grids. The top panels show the variability of resolution for both grids. The bottom panel shows the grid face edges for C180-global and C180e-US, with the 100 km, 250 km, and 500 km resolution contours for C180e-US.

heterogeneity in sources and topography that has challenged global models. The stretched-grid simulation, C900e-CA, has a grid size of C90 and stretch parameters $S = 10$, $\phi_t = 37.2\ ^\circ\mathrm{N}$, and $\theta_t = 119.5^\circ$ W. This simulation demonstrates that computationally, stretched-grid simulations are capable of very fine resolutions that are comparable to those of regional models. This experiment leverages the fine resolution of anthropogenic NO emissions from the NEI-2011 inventory ($0.1^\circ \times 0.1^\circ$ or $\sim$9 km). The meteorological data is conservatively downscaled from its native resolution of $0.25^\circ \times 0.3125^\circ$. This downscaling, along with all other regridding is performed online by ESMF. Work is underway in the GCHP–GMAO community to prepare finer resolution meteorological inputs for GEOS-Chem (including more vertical levels). Figure 7 shows the grids of C900e-CA and a nonstretched C90 cubed-sphere simulation, C90-global. The average resolution of C900e-CA in California is 11.2 km. The large stretch-factor used in C900e-CA causes some grid-boxes to expand significantly. Local scaling is useful for understanding the variability of the grid's resolution. For example, New York is approximately 4000 km from C900e-CA's target point. Figure 2 shows that for $S = 10$, the local scaling at 4000 km is close to 1. Equivalently, substituting $S = 10$ and $\Theta = 4000\ \mathrm{km}/\mathrm{r_E}$

https://doi.org/10.5194/gmd-2020-398
Preprint. Discussion started: 16 December 2020

Geoscientific Model Development Discussions
Open Access
EGU

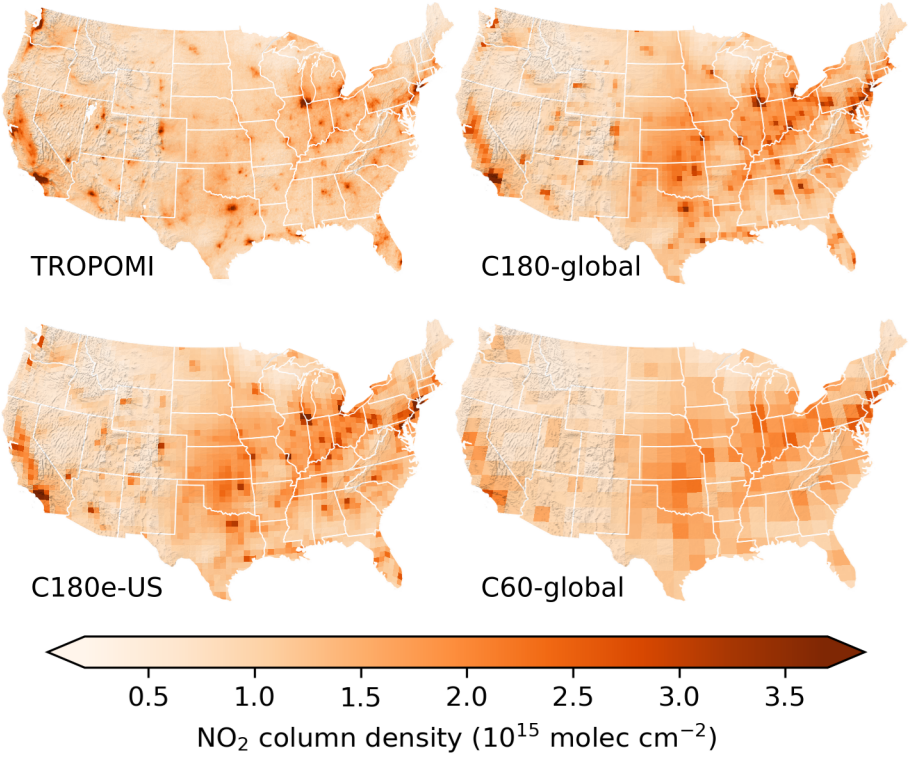

Figure 6. Mean tropospheric NO_2 column densities from C180-global, C180e-US, C60-global, and TROPOMI observations for July 2018. Simulated means only include points where TROPOMI observations were available. TROPOMI columns shown here use shape factors from C180e-US. TROPOMI columns with shape factors from C180-global were nearly identical.

Table 2. Timing test results comparing the computational expense of C180-global, C180e-US, and C60-global.

		C180-global	C180e-US	C60-global
Number of cores	(CPUs)	384	48	48
Wall times				
Chemistry	(hours)	21.8	7.0	7.2
Dynamics	(hours)	3.1	1.7	1.7
Data Input	(hours)	0.5	1.8	0.3
Other	(hours)	0.3	0.2	0.2
Total wall time	(hours)	25.7	10.7	9.4
Total CPU time	(days)	411	21.3	18.7

https://doi.org/10.5194/gmd-2020-398
Preprint. Discussion started: 16 December 2020

Geoscientific Model Development
Discussions
Open Access
EGU

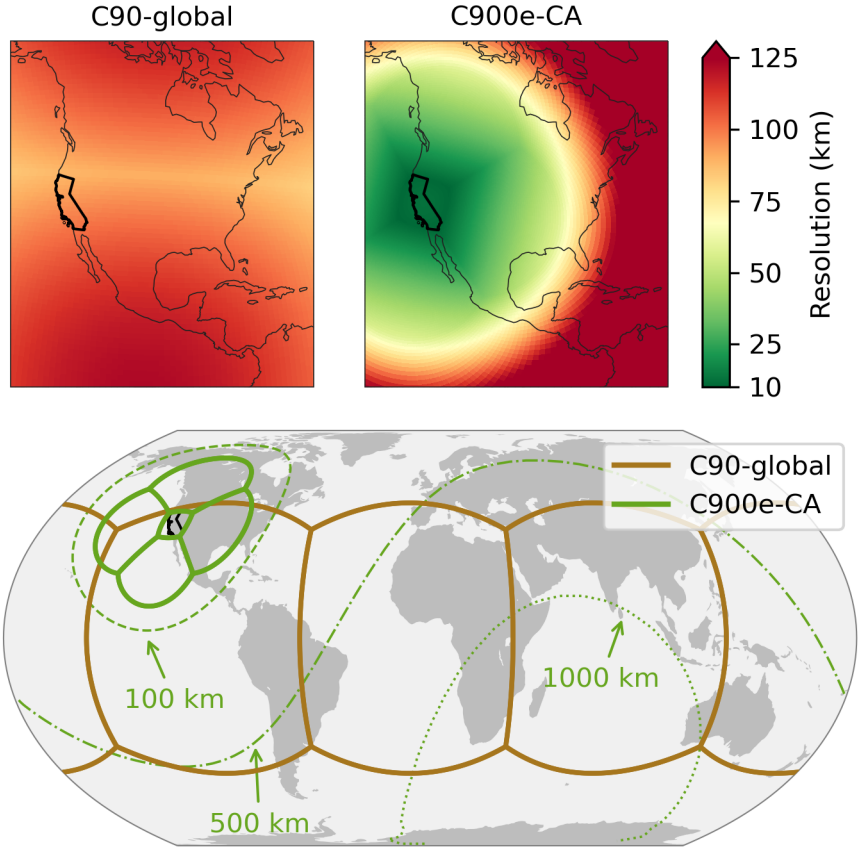

Figure 7. Comparison of C90-global and C900e-CA grids. The top panels show the variability of resolution for both grids. The bottom panel shows the grid face edges for C90-global and C900e-CA, with the 100 km, 500 km, and 1000 km resolution contours for C900e-CA.

in Eqn. 2 gives $L = 1.04$. Therefore, the resolution of C900e-CA in New York is similar to a nonstretched C90 cubed-sphere. This can be confirmed in Figure 7.

Figure 8 shows tropospheric NO_2 column densities from TROPOMI, C900e-CA, and C90-global for California in July 2018. The TROPOMI columns have significant fine-scale variability throughout California, high-concentrations over Los Angeles and in the San Francisco Bay Area, and smaller high-concentration features over Sacramento, Fresno, and Bakersfield. C900e-CA resolves many of the fine-scale spatial features seen in the TROPOMI columns, including the small high-concentration features over Sacramento, Fresno, and Bakersfield. The coarse resolution of C90-global fails to resolve most spatial features seen in the TROPOMI and C900e-CA columns, and significantly underestimates high concentrations except in Los Angeles (LA). A subtle feature in the TROPOMI columns is the strong gradient along the LA Basin perimeter. Neither simulation captures this gradient well, and LA's plume spuriously spreads into the Mojave Desert. The shallow inversion that prevents the plume from rising over the mountains might be better represented in finer resolution meteorological inputs that could better

https://doi.org/10.5194/gmd-2020-398
Preprint. Discussion started: 16 December 2020

Geoscientific Model Development Discussions
Open Access
EGU

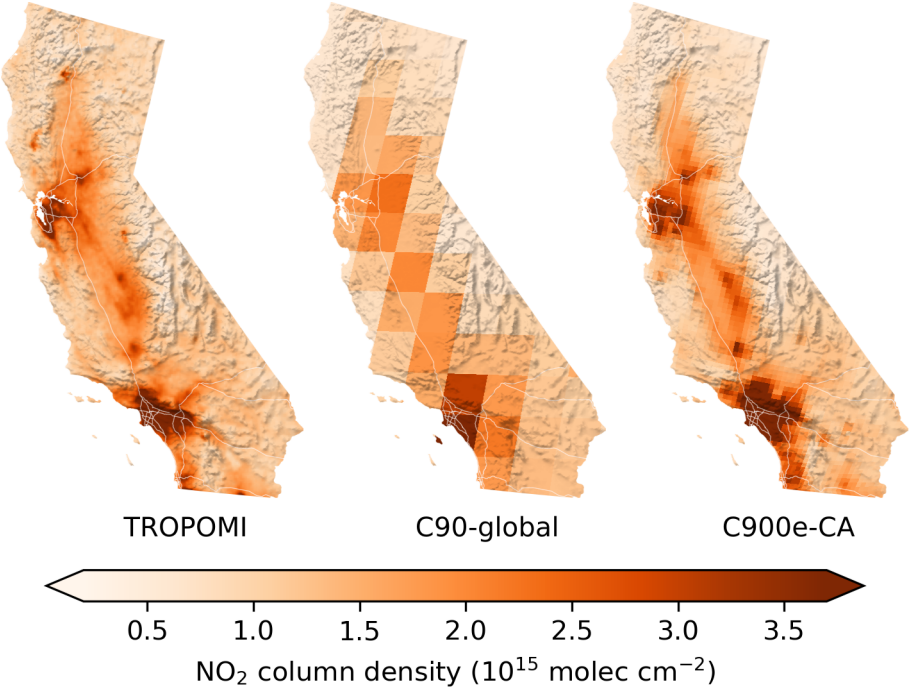

Figure 8. Mean tropospheric NO_2 column densities from C90-global, C900e-CA, and TROPOMI observations for July 2018. Simulated means only include points where TROPOMI observations were available. TROPOMI columns shown here use shape factors from C900e-CA.

capture sea breeze effects. Nonetheless, C900e-CA demonstrates a pronounced improvement over C90-global at resolving the challenging heterogeneity of California with similar computational expense (within 17 %).

4 Conclusions

Fine resolution simulations of atmospheric chemistry are necessary to capture fine-scale modes of variability such as localized sources, nonlinear chemistry, and boundary layer processes, but fine resolution simulations have been impeded by computational expense. This work developed stretched-grids for the high-performance implementation of GEOS-Chem (GCHP). The capability was validated against global cubed-sphere simulations, and applications were probed with case studies that compared simulated concentrations with observations from the TROPOMI satellite instrument.

Stretched-grids enable multiscale grids in GCHP and complement the other multiscale grid methods that are available in GEOS-Chem variants. The primary benefit of grid-stretching is ease of use. The refinement is flexible and controlled by four simple runtime parameters. Stretched-grids operate naturally in GCHP, so switching between stretched-grids and cubed-sphere grids is seamless. Stretched-grid simulations are standalone simulations, and do not require any pregenerated or dynamically-

https://doi.org/10.5194/gmd-2020-398
Preprint. Discussion started: 16 December 2020


Geoscientific Model Development Discussions
Open Access
EGU

coupled boundary conditions. Compared to nested grids, the main disadvantage of grid-stretching is that there is a single refinement, and that one cannot control the refined domain, refinement resolution, and global resolution independently.

Stretched-grid simulations can be used for regional- or continental-scale simulation purposes. Generally, stretch-factors in the range 1.4–4.0 are applicable for large refined domains. Higher stretch-factors can be used for very fine resolution simulations for regional-scale applications. To aid in choosing an appropriate stretch-factor, we propose a simple procedure based on choosing the maximum stretch-factor subject to two constraints: the size of the refinement, and the maximum and minimum resolution.

Computationally, stretched-grid simulations are capable of unprecedented spatial resolutions for GEOS-Chem. Improved emissions, with more accurate spatial and temporal variability, and meteorological inputs with finer horizontal, temporal, and vertical resolution are needed to fully exploit these newly achievable resolutions. Stretched-grids are publicly available and ready for scientific application in GEOS-Chem version 13.0.0.

Code availability. GEOS-Chem is an open source project distributed under the MIT License at https://github.com/geoschem/GCHP. The exact version of GCHP used in this manuscript was 13.0.0-alpha.3, and is archived on Zenodo (The International GEOS-Chem User Community, 2020).

https://doi.org/10.5194/gmd-2020-398
Preprint. Discussion started: 16 December 2020

Geoscientific Model Development Discussions
Open Access
EGU

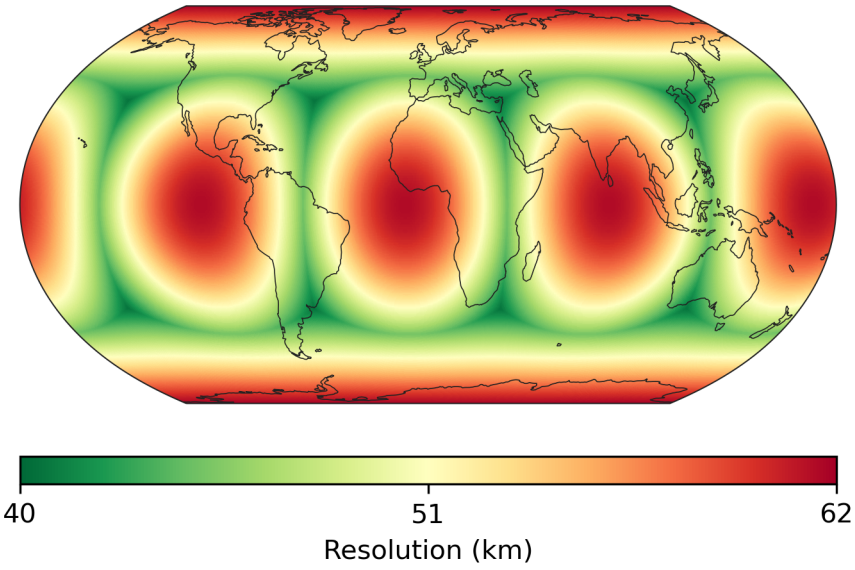

Figure A1. Variability of a C180 cubed-sphere's resolution.

Appendix A: Variability of cubed-sphere grid resolution

Figure A1 shows the variability of a C180 cubed-sphere grid's resolution. The coarsest resolutions is at the center of faces, and the finest resolutions are at the corners of the faces. The average resolution is 51.1 km. The resolution at the center of the face is 61.9 km (21.1 % greater than the average resolution). The resolution at the corner of the face is 40.6 km (25.8 % less than the average resolution).

Appendix B: Derivation of local scaling

Local scaling, L, is the relative change to a grid-box's length from grid-stretching. Consider a line segment that follows a meridian. The line segment starts at y and has length Δy. After remapping the line segment with the Schmidt transform (Eqn. 1), the line segment starts at y' and has length $\Delta y'$. The limit of the segment's local scaling as $\Delta y \to 0$ is equal to the derivative of the Schmidt transform:

$$L(y';S) = \lim_{\Delta y \to 0} \frac{\Delta y'}{\Delta y} = \lim_{\Delta y \to 0} \frac{\phi'(y+\Delta y) - \phi'(y)}{\Delta y} = \frac{\mathrm{d}}{\mathrm{d}y}\phi'(y) \tag{B1}$$

The derivative of the Schmidt transform is

$$\frac{\mathrm{d}}{\mathrm{d}y}\phi'(y) = \frac{2S}{S^2(1-\sin y)+\sin y+1} \tag{B2}$$

https://doi.org/10.5194/gmd-2020-398
Preprint. Discussion started: 16 December 2020


Geoscientific Model Development Discussions

so the local scaling at y' is

$$L(y';S) = \frac{2S}{S^2(1-\sin y)+\sin y+1} \tag{B3}$$

We can obtain the local scaling at y, rather than y', by substituting the inverse of the Schmidt transform into Eqn. B3. This gives

$$L(y;S) = \frac{S^2(1+\sin y)-\sin y+1}{2S} \tag{B4}$$

Finally, we can generalize Eqn. B5 so it is a function of arclength from the target. The center of the refinement after applying Eqn. 1 is at the South Pole. The arclength from y to the South Pole is $\Theta = y-(-\pi/2)$. Substituting $y = \Theta - \pi/2$ into Eqn. B5 gives

$$L(\Theta;S) = \frac{S^2(1-\cos\Theta)+\cos\Theta+1}{2S} \tag{B5}$$

Author contributions. LB implemented and validated the stretched-grid capability in GCHP. RVM, DJJ, and SP provided project oversight and top-level design. MJC reprocessed TROPOMI columns with shape factors from simulations. EWL, LB, and SDE performed MAPL 2 upgrade in GCHP. BMA and TLC developed stretched-grid capability in MAPL 2. HW, JL, LTM, and JM developed grid-independent emissions for GEOS-Chem, and CAK developed HEMCO. LB wrote the manuscript. All authors contributed to manuscript editing and revisions.

Competing interests. The authors declare that they have no conflict of interest.

Acknowledgements. This work was supported by a NASA AIST program grant (18-AIST18-0011), and by the Natural Sciences and Engineering Research Council of Canada (RGPIN-2019-04670).

https://doi.org/10.5194/gmd-2020-398
Preprint. Discussion started: 16 December 2020

Geoscientific Model Development Discussions

References

Bey, I., Jacob, D. J., Yantosca, R. M., Logan, J. A., Field, B. D., Fiore, A. M., Li, Q., Liu, H. Y., Mickley, L. J., and Schultz, M. G.: Global modeling of tropospheric chemistry with assimilated meteorology: Model description and evaluation, Journal of Geophysical Research: Atmospheres, 106, 23 073–23 095, https://doi.org/10.1029/2001JD000807, http://doi.wiley.com/10.1029/2001JD000807, 2001.

Boersma, K., Braak, R., and van der A, R. J.: Dutch OMI NO2 (DOMINO) data product v2. 0, Tropospheric Emissions Monitoring Internet Service on-line documentation, http://www.temis.nl/docs/OMI_NO2_HE5_2.0_2011.pdf, 2011.

Boersma, K. F., Eskes, H. J., Richter, A., De Smedt, I., Lorente, A., Beirle, S., van Geffen, J. H. G. M., Zara, M., Peters, E., Van Roozendael, M., Wagner, T., Maasakkers, J. D., van der A, R. J., Nightingale, J., De Rudder, A., Irie, H., Pinardi, G., Lambert, J.-C., and Compernolle, S. C.: Improving algorithms and uncertainty estimates for satellite NO $_2$ retrievals: results from the quality assurance for the essential climate variables (QA4ECV) project, Atmospheric Measurement Techniques, 11, 6651–6678, https://doi.org/10.5194/amt-11-6651-2018, https://www.atmos-meas-tech.net/11/6651/2018/, 2018.

Cooper, M. J., Martin, R. V., McLinden, C. A., and Brook, J. R.: Inferring ground-level nitrogen dioxide concentrations at fine spatial resolution applied to the TROPOMI satellite instrument, Environmental Research Letters, https://doi.org/10.1088/1748-9326/aba3a5, https://iopscience.iop.org/article/10.1088/1748-9326/aba3a5, 2020.

Davis, D. D., Grodzinsky, G., Kasibhatla, P., Crawford, J., Chen, G., Liu, S., Bandy, A., Thornton, D., Guan, H., and Sandholm, S.: Impact of ship emissions on marine boundary layer NO $_x$ and SO $_2$ Distributions over the Pacific Basin, Geophysical Research Letters, 28, 235–238, https://doi.org/10.1029/2000GL012013, http://doi.wiley.com/10.1029/2000GL012013, 2001.

Eastham, S. D., Long, M. S., Keller, C. A., Lundgren, E., Yantosca, R. M., Zhuang, J., Li, C., Lee, C. J., Yannetti, M., Auer, B. M., Clune, T. L., Kouatchou, J., Putman, W. M., Thompson, M. A., Trayanov, A. L., Molod, A. M., Martin, R. V., and Jacob, D. J.: GEOS-Chem High Performance (GCHP v11-02c): a next-generation implementation of the GEOS-Chem chemical transport model for massively parallel applications, Geoscientific Model Development, 11, 2941–2953, https://doi.org/10.5194/gmd-11-2941-2018, https://www.geosci-model-dev.net/11/2941/2018/, 2018.

Feng, X., Lin, H., and Fu, T.-M.: WRF-GC: online two-way coupling of WRF and GEOS-Chem for regional atmospheric chemistry modeling, other, pico, https://doi.org/10.5194/egusphere-egu2020-5165, https://meetingorganizer.copernicus.org/EGU2020/EGU2020-5165.html, 2020.

Fox-Rabinovitz, M., Côté, J., Dugas, B., Déqué, M., and McGregor, J. L.: Variable resolution general circulation models: Stretched-grid model intercomparison project (SGMIP), Journal of Geophysical Research, 111, D16 104, https://doi.org/10.1029/2005JD006520, http://doi.wiley.com/10.1029/2005JD006520, 2006.

Fox-Rabinovitz, M., Cote, J., Dugas, B., Deque, M., McGregor, J. L., and Belochitski, A.: Stretched-grid Model Intercomparison Project: decadal regional climate simulations with enhanced variable and uniform-resolution GCMs, Meteorology and Atmospheric Physics, 100, 159–178, https://doi.org/10.1007/s00703-008-0301-z, http://link.springer.com/10.1007/s00703-008-0301-z, 2008.

Freitas, S. R., Longo, K. M., Chatfield, R., Latham, D., Silva Dias, M. A. F., Andreae, M. O., Prins, E., Santos, J. C., Gielow, R., and Carvalho, J. A.: Including the sub-grid scale plume rise of vegetation fires in low resolution atmospheric transport models, Atmospheric Chemistry and Physics, 7, 3385–3398, https://doi.org/10.5194/acp-7-3385-2007, https://acp.copernicus.org/articles/7/3385/2007/, 2007.

Goldberg, D. L., Lamsal, L. N., Loughner, C. P., Swartz, W. H., Lu, Z., and Streets, D. G.: A high-resolution and observationally constrained OMI NO $_2$ satellite retrieval, Atmospheric Chemistry and Physics, 17, 11 403–11 421, https://doi.org/10.5194/acp-17-11403-2017, https://www.atmos-chem-phys.net/17/11403/2017/, 2017.

https://doi.org/10.5194/gmd-2020-398
Preprint. Discussion started: 16 December 2020

Griffin, D., Zhao, X., McLinden, C. A., Boersma, F., Bourassa, A., Dammers, E., Degenstein, D., Eskes, H., Fehr, L., Fioletov, V., Hayden, K., Kharol, S. K., Li, S., Makar, P., Martin, R. V., Mihele, C., Mittermeier, R. L., Krotkov, N., Sneep, M., Lamsal, L. N., Linden, M. t., Geffen, J. v., Veefkind, P., and Wolde, M.: High-Resolution Mapping of Nitrogen Dioxide With TROPOMI: First Results and Validation Over the Canadian Oil Sands, Geophysical Research Letters, 46, 1049–1060, https://doi.org/10.1029/2018GL081095, https://onlinelibrary.wiley.com/doi/abs/10.1029/2018GL081095, 2019.

Harris, L. M., Lin, S.-J., and Tu, C.: High-Resolution Climate Simulations Using GFDL HiRAM with a Stretched Global Grid, Journal of Climate, 29, 4293–4314, https://doi.org/10.1175/JCLI-D-15-0389.1, http://journals.ametsoc.org/doi/10.1175/JCLI-D-15-0389.1, 2016.

Heckel, A., Kim, S.-W., Frost, G. J., Richter, A., Trainer, M., and Burrows, J. P.: Influence of low spatial resolution a priori data on tropospheric NO $_2$ satellite retrievals, Atmospheric Measurement Techniques, 4, 1805–1820, https://doi.org/10.5194/amt-4-1805-2011, https://www.atmos-meas-tech.net/4/1805/2011/, 2011.

Hill, C., DeLuca, C., Balaji, Suarez, M., and Da Silva, A.: The Architecture of the Earth System Modeling Framework, Computing in Science & Engineering, 6, 18–28, https://doi.org/10.1109/MCISE.2004.1255817, http://ieeexplore.ieee.org/document/1255817/, 2004.

Hudman, R. C., Moore, N. E., Mebust, A. K., Martin, R. V., Russell, A. R., Valin, L. C., and Cohen, R. C.: Steps towards a mechanistic model of global soil nitric oxide emissions: implementation and space based-constraints, Atmospheric Chemistry and Physics, 12, 7779–7795, https://doi.org/10.5194/acp-12-7779-2012, https://acp.copernicus.org/articles/12/7779/2012/, 2012.

Ialongo, I., Virta, H., Eskes, H., Hovila, J., and Douros, J.: Comparison of TROPOMI/Sentinel-5 Precursor NO2 observations with ground-based measurements in Helsinki, Atmospheric Measurement Techniques, 13, 205–218, https://doi.org/10.5194/amt-13-205-2020, https://amt.copernicus.org/articles/13/205/2020/, 2020.

Keller, C. A., Long, M. S., Yantosca, R. M., Da Silva, A. M., Pawson, S., and Jacob, D. J.: HEMCO v1.0: a versatile, ESMF-compliant component for calculating emissions in atmospheric models, Geoscientific Model Development, 7, 1409–1417, https://doi.org/10.5194/gmd-7-1409-2014, https://www.geosci-model-dev.net/7/1409/2014/, 2014.

Kim, S.-W., Natraj, V., Lee, S., Kwon, H.-A., Park, R., de Gouw, J., Frost, G., Kim, J., Stutz, J., Trainer, M., Tsai, C., and Warneke, C.: Impact of high-resolution a priori profiles on satellite-based formaldehyde retrievals, Atmospheric Chemistry and Physics, 18, 7639–7655, https://doi.org/10.5194/acp-18-7639-2018, https://www.atmos-chem-phys.net/18/7639/2018/, 2018.

Li, J., Wang, Y., and Qu, H.: Dependence of Summertime Surface Ozone on NO $_x$ and VOC Emissions Over the United States: Peak Time and Value, Geophysical Research Letters, 46, 3540–3550, https://doi.org/10.1029/2018GL081823, https://onlinelibrary.wiley.com/doi/abs/10.1029/2018GL081823, 2019.

Li, Y., Henze, D. K., Jack, D., and Kinney, P. L.: The influence of air quality model resolution on health impact assessment for fine particulate matter and its components, Air Quality, Atmosphere & Health, 9, 51–68, https://doi.org/10.1007/s11869-015-0321-z, http://link.springer.com/10.1007/s11869-015-0321-z, 2016.

Li, Y., Pickering, K. E., Barth, M. C., Bela, M. M., Cummings, K. A., and Allen, D. J.: Evaluation of Parameterized Convective Transport of Trace Gases in Simulation of Storms Observed During the DC3 Field Campaign, Journal of Geophysical Research: Atmospheres, 123, 11,238–11,261, https://doi.org/10.1029/2018JD028779, http://doi.wiley.com/10.1029/2018JD028779, 2018.

Lin, H., Feng, X., Fu, T.-M., Tian, H., Ma, Y., Zhang, L., Jacob, D. J., Yantosca, R. M., Sulprizio, M. P., Lundgren, E. W., Zhuang, J., Zhang, Q., Lu, X., Zhang, L., Shen, L., Guo, J., Eastham, S. D., and Keller, C. A.: WRF-GC (v1.0): online coupling of WRF (v3.9.1.1) and GEOS-Chem (v12.2.1) for regional atmospheric chemistry modeling – Part 1: Description of the one-way model, Geoscientific Model Development, 13, 3241–3265, https://doi.org/10.5194/gmd-13-3241-2020, https://gmd.copernicus.org/articles/13/3241/2020/, 2020.

https://doi.org/10.5194/gmd-2020-398
Preprint. Discussion started: 16 December 2020

Long, M. S., Yantosca, R., Nielsen, J. E., Keller, C. A., da Silva, A., Sulprizio, M. P., Pawson, S., and Jacob, D. J.: Development of a grid-independent GEOS-Chem chemical transport model (v9-02) as an atmospheric chemistry module for Earth system models, Geoscientific Model Development, 8, 595–602, https://doi.org/10.5194/gmd-8-595-2015, https://gmd.copernicus.org/articles/8/595/2015/, 2015.

Lorente, A., Folkert Boersma, K., Yu, H., Dörner, S., Hilboll, A., Richter, A., Liu, M., Lamsal, L. N., Barkley, M., De Smedt, I., Van Roozendael, M., Wang, Y., Wagner, T., Beirle, S., Lin, J.-T., Krotkov, N., Stammes, P., Wang, P., Eskes, H. J., and Krol, M.: Structural uncertainty in air mass factor calculation for NO $_2$ and HCHO satellite retrievals, Atmospheric Measurement Techniques, 10, 759–782, https://doi.org/10.5194/amt-10-759-2017, https://www.atmos-meas-tech.net/10/759/2017/, 2017.

Mari, C., Jacob, D. J., and Bechtold, P.: Transport and scavenging of soluble gases in a deep convective cloud, Journal of Geophysical Research: Atmospheres, 105, 22 255–22 267, https://doi.org/10.1029/2000JD900211, http://doi.wiley.com/10.1029/2000JD900211, 2000.

McDuffie, E., Smith, S., O'Rourke, P., Tibrewal, K., Venkataraman, C., Marais, E., Zheng, B., Crippa, M., Brauer, M., and Martin, R.: CEDS_GBD-MAPS: Global Anthropogenic Emission Inventory of NOx, SO2, CO, NH3, NMVOCs, BC, and OC from 1970-2017, https://doi.org/10.5281/ZENODO.3754964, https://zenodo.org/record/3754964, version Number: 2020_v1.0 type: dataset, 2020.

Murray, L. T., Jacob, D. J., Logan, J. A., Hudman, R. C., and Koshak, W. J.: Optimized regional and interannual variability of lightning in a global chemical transport model constrained by LIS/OTD satellite data: IAV OF LIGHTNING CONSTRAINED BY LIS/OTD, Journal of Geophysical Research: Atmospheres, 117, https://doi.org/10.1029/2012JD017934, http://doi.wiley.com/10.1029/2012JD017934, 2012.

Palmer, P. I., Jacob, D. J., Chance, K., Martin, R. V., Spurr, R. J. D., Kurosu, T. P., Bey, I., Yantosca, R., Fiore, A., and Li, Q.: Air mass factor formulation for spectroscopic measurements from satellites: Application to formaldehyde retrievals from the Global Ozone Monitoring Experiment, Journal of Geophysical Research: Atmospheres, 106, 14 539–14 550, https://doi.org/10.1029/2000JD900772, http://doi.wiley.com/10.1029/2000JD900772, 2001.

Punger, E. M. and West, J. J.: The effect of grid resolution on estimates of the burden of ozone and fine particulate matter on premature mortality in the USA, Air Quality, Atmosphere & Health, 6, 563–573, https://doi.org/10.1007/s11869-013-0197-8, http://link.springer.com/10.1007/s11869-013-0197-8, 2013.

Putman, W. M. and Lin, S.-J.: Finite-volume transport on various cubed-sphere grids, Journal of Computational Physics, 227, 55–78, https://doi.org/10.1016/j.jcp.2007.07.022, https://linkinghub.elsevier.com/retrieve/pii/S0021999107003105, 2007.

Schmidt, F.: Variable fine mesh in spectral global models, Beitr. Phys. Atmos., 50, 211–217, 1977.

Stettler, M., Eastham, S., and Barrett, S.: Air quality and public health impacts of UK airports. Part I: Emissions, Atmospheric Environment, 45, 5415–5424, https://doi.org/10.1016/j.atmosenv.2011.07.012, https://linkinghub.elsevier.com/retrieve/pii/S135223101100728X, 2011.

Suarez, M., Trayanov, A., Hill, C., Schopf, P., and Vikhliaev, Y.: MAPL: a high-level programming paradigm to support more rapid and robust encoding of hierarchical trees of interacting high-performance components, in: Proceedings of the 2007 symposium on Component and framework technology in high-performance and scientific computing - CompFrame '07, p. 11, ACM Press, Montreal, Quebec, Canada, https://doi.org/10.1145/1297385.1297388, http://portal.acm.org/citation.cfm?doid=1297385.1297388, 2007.

Tack, F., Merlaud, A., Iordache, M.-D., Pinardi, G., Dimitropoulou, E., Eskes, H., Bomans, B., Veefkind, P., and Van Roozendael, M.: Assessment of the TROPOMI tropospheric NO2 product based onairborne APEX observations, preprint, Gases/Remote Sensing/Validation and Intercomparisons, https://doi.org/10.5194/amt-2020-148, https://amt.copernicus.org/preprints/amt-2020-148/, 2020.

The International GEOS-Chem User Community: geoschem/geos-chem: GEOS-Chem 12.5.0, https://doi.org/10.5281/ZENODO.3403111, https://zenodo.org/record/3403111, 2019.

The International GEOS-Chem User Community: geoschem/gchp: GCHP 13.0.0-alpha.3, https://doi.org/10.5281/ZENODO.4317978, https://zenodo.org/record/4317978, 2020.

https://doi.org/10.5194/gmd-2020-398
Preprint. Discussion started: 16 December 2020

Geoscientific Model Development Discussions

Thompson, M., Auer, B., Clune, T., Trayanov, A., Jiang, W., Norris, P., Lundgren, L., Sherman, E., Jamieson, W., Bindle, L., Eastham, S. D., Putman, B., and Vikhliaev, Y.: GEOS-ESM/MAPL: MAPL 2.2 Release, https://doi.org/10.5281/ZENODO.3903435, https://zenodo.org/record/3903435, 2020.

Valin, L. C., Russell, A. R., Hudman, R. C., and Cohen, R. C.: Effects of model resolution on the interpretation of satellite NO_2 observations, Atmospheric Chemistry and Physics, 11, 11 647–11 655, https://doi.org/10.5194/acp-11-11647-2011, https://www.atmos-chem-phys.net/11/11647/2011/, 2011.

Veefkind, J., Aben, I., McMullan, K., Förster, H., de Vries, J., Otter, G., Claas, J., Eskes, H., de Haan, J., Kleipool, Q., van Weele, M., Hasekamp, O., Hoogeveen, R., Landgraf, J., Snel, R., Tol, P., Ingmann, P., Voors, R., Kruizinga, B., Vink, R., Visser, H., and Levelt, P.: TROPOMI on the ESA Sentinel-5 Precursor: A GMES mission for global observations of the atmospheric composition for climate, air quality and ozone layer applications, Remote Sensing of Environment, 120, 70–83, https://doi.org/10.1016/j.rse.2011.09.027, https://linkinghub.elsevier.com/retrieve/pii/S0034425712000661, 2012.

Wang, Y. X., McElroy, M. B., Jacob, D. J., and Yantosca, R. M.: A nested grid formulation for chemical transport over Asia: Applications to CO: NESTED GRID CO SIMULATION OVER ASIA, Journal of Geophysical Research: Atmospheres, 109, https://doi.org/10.1029/2004JD005237, http://doi.wiley.com/10.1029/2004JD005237, 2004.

Weng, H., Lin, J., Martin, R., Millet, D. B., Jaeglé, L., Ridley, D., Keller, C., Li, C., Du, M., and Meng, J.: Global high-resolution emissions of soil NOx, sea salt aerosols, and biogenic volatile organic compounds, Scientific Data, 7, 148, https://doi.org/10.1038/s41597-020-0488-5, http://www.nature.com/articles/s41597-020-0488-5, 2020.

Yan, Y.-Y., Lin, J.-T., Kuang, Y., Yang, D., and Zhang, L.: Tropospheric carbon monoxide over the Pacific during HIPPO: two-way coupled simulation of GEOS-Chem and its multiple nested models, Atmospheric Chemistry and Physics, 14, 12 649–12 663, https://doi.org/10.5194/acp-14-12649-2014, https://www.atmos-chem-phys.net/14/12649/2014/, 2014.

Zhao, X., Griffin, D., Fioletov, V., McLinden, C., Cede, A., Tiefengraber, M., Müller, M., Bognar, K., Strong, K., Boersma, F., Eskes, H., Davies, J., Ogyu, A., and Lee, S. C.: Assessment of the quality of TROPOMI high-spatial-resolution NO2 data products in the Greater Toronto Area, Atmospheric Measurement Techniques, 13, 2131–2159, https://doi.org/10.5194/amt-13-2131-2020, https://amt.copernicus.org/articles/13/2131/2020/, 2020.

Zhuang, J., Jacob, D. J., Lin, H., Lundgren, E. W., Yantosca, R. M., Gaya, J. F., Sulprizio, M. P., and Eastham, S. D.: Enabling High-Performance Cloud Computing for Earth Science Modeling on Over a Thousand Cores: Application to the GEOS-Chem Atmospheric Chemistry Model, Journal of Advances in Modeling Earth Systems, 12, https://doi.org/10.1029/2020MS002064, https://onlinelibrary.wiley.com/doi/abs/10.1029/2020MS002064, 2020.